

Copper-binding properties of microplastic-derived dissolved organic matter revealed by fluorescence spectroscopy and two-dimensional correlation spectroscopy[☆]

Yun Kyung Lee^a, Seongjin Hong^b, Jin Hur^{a,*}

^a Department of Environment and Energy, Sejong University, 209 Neungdong-ro, Gwangjin-gu, Seoul 05006, South Korea

^b Department of Ocean Environmental Sciences, Chungnam National University, Daejeon, 34134, South Korea

ARTICLE INFO

Article history:

Received 17 October 2020

Revised 17 December 2020

Accepted 20 December 2020

Available online 23 December 2020

Keywords:

Microplastics

Dissolved organic matter

Copper binding

Fluorescence quenching

EEM-PARAFAC

Two-dimensional correlation spectroscopy

ABSTRACT

Despite numerous studies on microplastics (MPs), little attention has been paid to the dissolved organic substances leached from MPs and their environmental fate. In this study, we explored the copper-binding characteristics of MP-derived dissolved organic matter (MP-DOM) leached from several MP types, including commercial polypropylene, polyvinylchloride, and expanded polystyrene, under dark and UV irradiation conditions. The copper-binding affinity of MP-DOM was examined using fluorescence quenching method based on different fluorophores identified via the excitation emission matrix-parallel factor analysis (EEM-PARAFAC). The heterogeneous distribution of binding sites across the functional groups of MP-DOM was further elucidated by utilizing two-dimensional correlation spectroscopy (2D-COS) based on Fourier transform infrared spectroscopy (FTIR). Phenol/protein-like fluorescence prevailed in all MP-DOM samples, whereas humic-like fluorescence was more pronounced in the irradiated MP-DOM. For all tested plastic types, two plastic-derived fluorescent components (C2 and C3) exhibited substantial fluorescence quenching with increasing copper concentrations. The calculated stability constants showed larger differences between the two leaching conditions than between the three MP types with higher $\log K_M$ values for the UV-irradiated (4.08–5.36) than dark-treated MP-DOM (1.05–3.60). The binding constants were comparable to those of natural organic matter with aquatic/terrestrial origins. The 2D-COS results further revealed that the oxygen-containing structures in MP-DOM generated by UV irradiation might be responsible for the higher binding affinity of the irradiated MP-DOM. This is the first study demonstrating the environmental reactivity of MP-DOM towards metal binding, highlighting the importance of leaching conditions for the metal-binding behavior of MP-DOM.

© 2020 Elsevier Ltd. All rights reserved.

1. Introduction

Owing to the massive production of plastic and its incorrect disposal, micro-sized plastic particles (so-called microplastics, MPs) pose a great risk to aquatic ecosystems (He et al., 2018; Syberg et al., 2015). Many studies have investigated the occurrence and fate of MPs in aquatic/terrestrial environments from various aspects (Eerkes-Medrano et al., 2015; Van Cauwenberghe et al., 2015; Wang et al., 2019). Recent studies have revealed that MPs can release a substantial amount of dissolved organic substances, so-called MP-derived dissolved organic matter (MP-DOM), when they are in contact with water (Lee et al., 2020c; Romera-Castillo et al., 2018). MP-DOM comprises multiple organic com-

pounds such as additives and various chain scission products from the main polymers including bisphenol, phthalates, and styrene as monomer of PS plastics (Gewert et al., 2018; Suhrhoff and Scholz-Böttcher, 2016). In aquatic systems, MPs may undergo a series of weathering processes, including turbulence by wave and/or exposure to UV light, which can facilitate the release of MP-DOM into their surroundings (Potthoff et al., 2017).

Of the weathering processes that affect the release of MP-DOM, UV irradiation can be considered as a strong driver for the production of MP-DOM from plastic particles (Lee et al., 2020c; Potthoff et al., 2017). It was previously reported that MP-DOM leached under UV irradiation contained more abundance of oxygen-containing groups (e.g., carboxylic and/or phenolic groups) and more pronounced humic-like fluorescence compared to those under dark condition (Galgani et al., 2018; Lee et al., 2020b) although the specific features of MP-DOM depended on the plastic type and leaching conditions (Galgani et al., 2018; Lee et al.,

[☆] Revised and Re-submitted to *Water Research*, December 2020

* Corresponding author.

E-mail address: jinhur@sejong.ac.kr (J. Hur).

2020b). Furthermore, recent literature has shown that MP-DOM could have observable environmental reactivities at levels similar to natural organic matter (NOM) in terms of their tendency to adsorb onto minerals and disinfection byproduct precursors (Lee and Hur, 2020; Lee et al., 2020c).

The interaction of DOM with trace metals is considered to be a critical factor in determining the fate, mobility, and toxicity of metals in aqueous systems (de Polo and Scrimshaw, 2012; Santore et al., 2001). Under the chemistry of fixed solution, the extent of metal binding is heavily impacted by the chemical composition and structures of DOM. Numerous studies have shown that carboxylic and phenolic groups in DOM serve as effective binding sites/ligands for metals (Croué et al., 2003; Shi et al., 2016). As fluorescence spectroscopy is a fast, highly sensitive, and cost-effective measurement technique, the metal-binding property of DOM has been frequently studied using the fluorescence quenching method (FQM) (Wang et al., 2015; Wu et al., 2004). In the FQM, a 1:1 metal-ligand complex is assumed (Hays et al., 2004; Ryan and Weber, 1982) and the binding constants are estimated by applying the Ryan–Weber model or the Stern–Volmer equation. The metal-binding characteristics of DOM can be further examined with respect to the heterogeneous distribution of binding sites in bulk DOM. For example, metal-binding affinities of different fluorophores within bulk DOM have been estimated by applying the FQM on different components identified using the parallel factor analysis (PARAFAC) model on the fluorescence excitation emission matrix (EEM) (Song et al., 2017a; Xu et al., 2013a; Yamashita and Jaffé, 2008). Two-dimensional correlation spectroscopy (2D-COS) has been coupled with fluorescence spectroscopy (Hur and Lee, 2011; Lee et al., 2020a) or Fourier transform infrared spectroscopy (FTIR) (Huang et al., 2018; Li et al., 2017) to further investigate the complex interactions between metals and DOM.

Fluorescence spectroscopy has been long used to determine the distributions of different fluorophores in DOM samples (Brogi et al., 2020; Coble, 1996). The peak locations and intensities of detected fluorophores have been associated with different chemical composition and molecular sizes (Yang et al., 2015). FTIR can offer the information on relative abundances of basic functional groups contained in DOM samples. Both tools have gained popularity for easily exploring the variations of DOM characteristics due to their preferred merits such as fast measurements, low cost, and minimal sample treatment. In particular, they have been widely employed to examine the interactions between DOM and metals (Huang et al., 2018; Plaza et al., 2006; Yamashita and Jaffé, 2008). The two methods are complementary to each other for DOM characterization in that FTIR is a qualitative method but can reveal non-fluorescent structures while fluorescence spectroscopy gives the quantitative estimation of specific fluorescent components.

Previous studies have revealed that MP-DOM has fluorescence properties as well as complex functional groups (Lee and Hur, 2020; Lee et al., 2020c). This feature is similar to NOM. In the context, whether MP-DOM behaves similar to NOM in its interactions with trace metals in the environment is an interesting and challenging question of environmental significance. No previous study has examined the interactions between MP-DOM and trace metals. Furthermore, the information regarding the interaction of MP-DOM with metals is essential for understanding the fate and transport of metals in MPs-polluted environments where the release of MP-DOM from plastic particles is likely to occur. Thus, this study specifically aimed to (1) characterize MP-DOM obtained under two different leaching conditions (dark and UV irradiation) and from three plastic types (PP, PVC, and EPS) via measurements of dissolved organic carbon (DOC), fluorescence EEM, and FTIR analyses; (2) explore the binding behaviors of different fluorescent components within bulk MP-DOM towards copper; (3) apply 2D-COS

to elucidate the potentially complex interactions involving various functional groups; and (4) compare the binding stability constants of MP-DOM with those of aquatic/terrestrial NOM.

2. Materials and methods

2.1. Preparation for MP-DOM samples

2.1.1. Microplastics

In this study, polypropylene (PP), polyvinylchloride (PVC), and expanded polystyrene (EPS) were selected as representative plastic types. Commercial plastics were purchased in sheet form (1 mm in thickness) for PP and PVC and as beads (1 mm in diameter) for EPS from a local market in Seoul, South Korea. Plastics were cut into pieces of approximately 1 mm × 1 mm, and the cut pieces were sufficiently washed with distilled water to remove any impurities that might have been introduced during the cutting process.

2.1.2. Leaching experiments

Leaching experiments were conducted for 14 days with an artificial freshwater solution containing 5.0 g/L plastic pieces under two different experimental conditions (i.e., dark and UV irradiation). The added plastic dose (i.e., 5 g/L) was determined based on the ranges used in other similar studies (Lee and Hur, 2020; Suhrhoff and Scholz-Böttcher, 2016). As the main goal of this study was to characterize the metal-binding properties of MP-DOM, the MP doses were intentionally set at a relatively higher level compared to those typically observed in natural environments (Alimi et al., 2018; Chae and An, 2018). The total number of MP pieces was additionally estimated by taking into account the average weight of one piece, which was 1,316 pieces for PP, 649 pieces for PVC, and 48,387 pieces for EPS (Table S1). The leaching solution consisted of NaHCO₃ (96 mg/L), CaSO₄ (47.4 mg/L), MgSO₄•7H₂O (122.86 mg/L), and KCl (4 mg/L), which mimics the ion composition of typical freshwater (Majedi et al., 2014). The MP pieces were added to the artificial freshwater solution (1 L) in a sterilized amber glass bottle before the solution was placed on a shaker at 150 rpm during the 14 days of leaching in the dark.

For the UV irradiation setup, the MP-containing freshwater solution was transferred into a quartz tube that was previously autoclaved at 120 °C for 15 min. The tube was placed in the center of a closed cabinet equipped with six 8 W UVA lamps (Sankyo Denki, F8T5BL) as a light source (Lee et al., 2020c). A stirrer was placed at the bottom of the quartz tube to maintain continuous mixing throughout the leaching period. At the end of leaching, the mixing solution was filtered through pre-ashed Whatman GF/F filters to obtain the MP-DOM samples. For this step, a glass vacuum filtration device was used to avoid contact with extraneous plastic materials. As representative NOM materials for comparison, Suwanee River fulvic acid (SRFA) and Elliott Soil humic acid (ESHA) were purchased from the International Humic Substances Society. The NOM stock solutions were prepared by dissolving 10 mg of the powder in 1 L of Milli-Q water, which resulted in concentrations of 6.4 mg-C/L for SRFA and 4.5 mg-C/L for ESHA.

2.2. Determination of copper complexing capacities and stability constants

Prior to the copper-binding experiments, the MP-DOM and NOM solutions were diluted such that the three types of MP-DOM samples (i.e., PP-, PVC-, and EPS-DOM) had identical DOC concentration (i.e., ~0.25 mg-C/L), which was the same as the concentration of PP-DOM (Fig. S1). Copper was used as a representative metal in this study because it has been previously studied for metal-DOM interactions; thus, the results can be easily compared with those of previous studies (Hu et al., 2017; Yamashita and Jaffé,

2008). The copper stock solutions were prepared by dissolving different amounts of $\text{Cu}(\text{NO}_3)_2$ in Milli-Q water to obtain copper concentrations of 0.2, 1.0, and 5.0 mM. The DOM solutions, either MP-DOM or NOM, were transferred into polytetrafluorethylene (PTFE) vials (20 mL). The copper stock solutions were then spiked into the DOM-containing vials to obtain final copper concentrations varying from 5 to 200 μM (Hur and Lee, 2011; Lee and Hur, 2017). The total volume was kept the same (20 mL). The vials were then placed on a shaker at 150 rpm and allowed to equilibrate for 15 min. As significant DOM leaching was not observed from the PTFE vial containing only the copper solution, it was considered as a blank (Fig. S2b).

Fluorescence quenching models such as the Ryan–Weber model and the modified Stern–Volmer equation have been widely applied to calculate the parameters related to the metal-binding behavior of DOM (Guo et al., 2019; Hur and Lee, 2011). Although the models have the inherent limitation of not being able to fully characterize metal-DOM interactions, which arises from the simple assumption of 1:1 complexation, they are still popular owing to the advantages of easy and fast measurements. In this study, we adopted the modified Stern–Volmer equation as a fluorescence quenching model, where nonlinear fluorescence responses to metal binding are considered to estimate the relative portions of unquenched fluorophores (da Silva et al., 1998; Hays et al., 2004). The model parameters related to binding affinity and relative abundance of binding sites were calculated based on the following equation:

$$F_0/(F_0 - F) = 1/(f \cdot K_M \cdot C_M) + 1/f \quad (1)$$

where F , F_0 , f , and C_M refer to the measured fluorescence intensity, the initial fluorescence intensity, the fraction of the fluorophores participating in binding, and Cu^{2+} concentration, respectively. The conditional stability constant, K_M , was estimated from the slope of $F_0/(F_0 - F)$ against $1/C_M$.

2.3. Analytical measurements

2.3.1. DOC and FTIR spectroscopy

The DOC concentrations of the samples were determined using a TOC analyzer (Shimadzu L-series, TOC-CHP, Japan). The samples for DOC analyses were collected in pre-combusted 40 mL glass vials. They were acidified with 1 M HCl solution to a pH of ~2.0 to minimize biodegradation and were stored at 4 °C until measurement.

FTIR spectroscopy (Nicolet iS10, Thermo Scientific, USA) was used to identify the functional groups present in the MP-DOM samples. The detailed procedure for FTIR analysis is available in other reports (Chen et al., 2018; Lee et al., 2020c). In brief, 10 mL of a filtered MP-DOM sample was mixed with 100 mg of KBr powder (Sigma Aldrich, FTIR grade) and freeze-dried for further analysis. As a blank, clean KBr pellets were prepared by drying at 105 °C for 2 h. The scanned wavenumber range was between 650 and 4000 cm^{-1} . Each FTIR spectrum was corrected for baseline shifts and smoothed using Origin 9.0 software (12 points, Savitzky–Golay method). The FTIR peak intensities were normalized by the summed intensities of all the observed peaks (Yang et al., 2015).

2.3.2. Fluorescence EEM measurements and PARAFAC modeling

Fluorescence EEM spectra were obtained using a fluorescence spectrophotometer (F-7000, Hitachi, Japan). The scan was run at an emission wavelength (Em) from 280 to 550 nm with steps of 1 nm. The excitation wavelengths (Ex) for the emission scan were varied in the range of 220–500 nm with a stepwise increment of 5 nm. The excitation and emission slits were adjusted to 10 nm. The fluorescence response to Milli-Q water was taken into account as a blank to obtain the final EEM data of DOM samples through

subtraction. The fluorescence intensities were normalized to Raman units (R.U.) using the intensity of the integrated Raman peak at 350 nm (Em) (Lawaetz and Stedmon, 2009).

PARAFAC modeling was performed using MATLAB 7.0 (Mathworks, Natick, MA, USA) along with the drEEM Toolbox (Murphy et al., 2013). The number of independent fluorescent DOM (FDOM) components was determined using split-half validation of the EEM results obtained from copper binding experiment and the percentage of the explained variance (95.2%). The maximum fluorescence intensities (F_{max}) of the identified FDOM components were adopted to represent the relative quantities of the individual components. In this study, the EEM data of NOM samples were also incorporated into the modeling to directly compare MP-DOM and NOM samples.

2.3.3. 2D-COS

2D-COS was applied to identify sequential changes occurring in the FTIR spectra of MP-DOM caused by the addition of copper as an external perturbation. Typically, the procedure generates two types of two-dimensional maps called synchronous and asynchronous maps, which were obtained using an open-access software (2D-Shige version 1.3, <https://sites.google.com/site/Shigemorita/home/2dshige>). In the synchronous map, auto peaks, which appear on the diagonal line, indicate spectral changes due to the addition of copper and their locations. Cross-peaks located off the diagonal line represent simultaneous changes of the variables occurring at two different locations (i.e., x- and y-axis). Positive cross-peaks imply that the changes occur in the same direction for the two variables, whereas negative cross-peaks imply that the changes are in opposite directions. On the other hand, cross-peaks in the asynchronous map provide information on the sequence of changes. The interpretation is entirely based on Noda's rule (Noda and Ozaki, 2005). According to the rule, if the signs of cross-peaks (positive or negative) are the same in both types of maps, the signal change on the x-axis precedes that on the y-axis, whereas the order of the sequence is reversed if the signs of peaks on the two maps are opposite. The mathematical expressions for the 2D-COS and map generation are described elsewhere (Noda, 2016; Park et al., 2016).

3. Results and discussion

3.1. Basic characteristics of MP-DOMs

3.1.1. Functional groups

The MPs used in this study presented distinct features in the FTIR spectra for the individual plastic types with the appearance of four peaks for PP (designated as peaks A, C, D, and G), five peaks for PVC (designated as peaks A', E', F', G', and J'), and six peaks for EPS (designated as peaks A'', B'', F'', G'', H'', and I'') (Fig. 1a and Table S2). Some of the peaks originate from carbon chains consisting of repeating C–H units, which correspond to peaks A and C for PP, peaks A' and E' for PVC, and peaks B'' and G'' for EPS. Peaks have also been observed in other plastic types such as polyethylene (PE) and PP in a previous study (Jung et al., 2018). In this study, PP and EPS types were well discriminated by the exclusive presence of peaks D and G for PP and peaks A' and F'' for EPS. No chlorine-related peak was observed in the PVC particles in the present study, although a few prior studies reported the presence of a unique peak for PVC (Noda et al., 2007; Verleye et al., 2001).

For the MP-DOM samples, the peaks of C–H bands were observed in the FTIR spectra as a common plastic proxy (e.g., peaks A, A', or B'') independent of the plastic types and leaching conditions. Similar observations were previously reported for MP-DOM derived from PE and PP polymer materials (Lee et al., 2020c). Additionally, new peaks were identified from the MP-DOM samples,

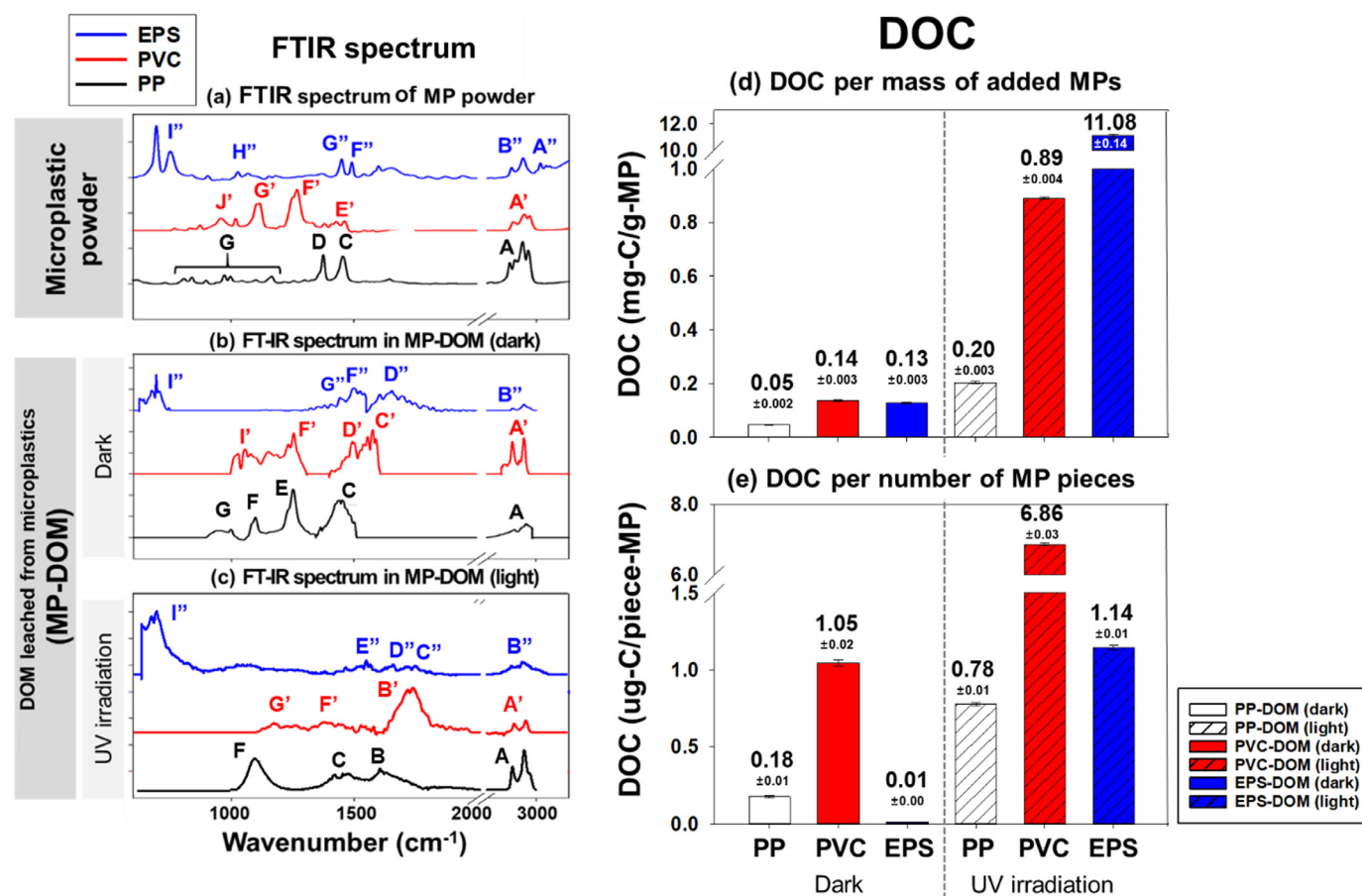


Fig. 1. Basic characteristics of leached DOM from PP, PVC, and EPS plastics after 14 days of leaching (5 g-MP/L) under dark and UV irradiation conditions. FTIR spectra of (a) MP particles and MP-DOM under (b) dark and (c) UV irradiation conditions. DOC concentrations of MP-DOM (d) per added mass of plastics and (e) per number of MP pieces. The letters in the IR spectra represent the main absorption bands (cm⁻¹) associated with the corresponding plastic structures in Table S2. Information on the estimation of the number of MP pieces is presented in Table S1.

which were not observed in the MP particles. For example, peaks C' and D', which are related to additives, emerged in the spectra of the dark-treated PVC-DOM, while peak D'', which represents the monomers of EPS, appeared in the leached DOM from EPS plastic under dark conditions (Fig. 1b). For the UV-treated MP-DOM samples, additional features were observed with the appearance of peaks B' and G' for PVC-DOM and peaks C'' and E'' for EPS-DOM (Fig. 1c). No oxygen-containing functional groups were found for the irradiated PP-DOM. Unique peaks of the UV-irradiated MP-DOM samples have been reported for other oxidized polymers (Gugumus, 1999; Lucki and Rånby, 1979), which suggested that the new peaks might be associated with oxygen-containing compounds generated by photo-oxidation via UV irradiation (Table S2). The FTIR results of the irradiated MP-DOM are in line with those from a previous study employing mass spectroscopy that provided molecular evidence of the release of polymer fragments with oxidized end groups into the aqueous phase from PET and EPS plastics after exposure to UV light (Gewert et al., 2018).

3.1.2. Concentration of leached DOC

Under dark conditions, the released DOC concentrations per gram of PVC or EPS were more than two-fold higher than that from PP (0.140 ± 0.003 mg-C/g-PVC and 0.130 ± 0.003 mg-C/g-EPS versus 0.050 ± 0.002 mg-C/g-PP) (Fig. 1d). The results suggested that the amounts of leached DOC might be highly dependent on the plastic type. PVC and EPS plastics contain a relatively high content of additives than PP, and the additives can be leached to a greater extent by close contact with the aqueous phase than

the main plastic structures such as polymers (Hermabessiere et al., 2017; Jang et al., 2017). The leached amounts of MP-DOM per plastic mass were much greater for the UV-irradiated samples than those for the dark-treated samples. For example, after 14 days of irradiation, the DOC concentration per mass of EPS-DOM was more than 80 times higher than that under dark conditions, which implies that UV irradiation could play a role in changing plastic surfaces into structures vulnerable to dissolution (Gardette et al., 2013). In this study, the high leaching tendency of MP-DOM upon UV stimulation was more pronounced for PVC than for PP and EPS with leached concentrations of 11.08 ± 0.14 , 0.20 ± 0.003 and 0.89 ± 0.004 mg-C/g, respectively, at the end of the UV irradiation. The structural instability of EPS under UV irradiation was also reported in a previous study (Song et al., 2017b), in which a significant difference was observed in the number of fragmented plastic particles with and without 6-month-long exposure to UV light ($12,152 \pm 3,276$ particles per pellet under light versus $4,220 \pm 33$ particles per pellet in the dark).

Similar to the DOC concentration per added mass, the leached quantities of MP-DOM per number of plastic pieces also showed clear differences among the different plastic types (Fig. 1e). For example, under dark conditions, the DOC concentration per number of PVC pieces was nearly 100 times higher than that of EPS. This trend agrees well with a previous report (Suhroff and Scholz-Böttcher, 2016), showing that the amount of released additives per surface area of PVC in the dark was nearly ten times greater than that released by PS. This result is noteworthy considering

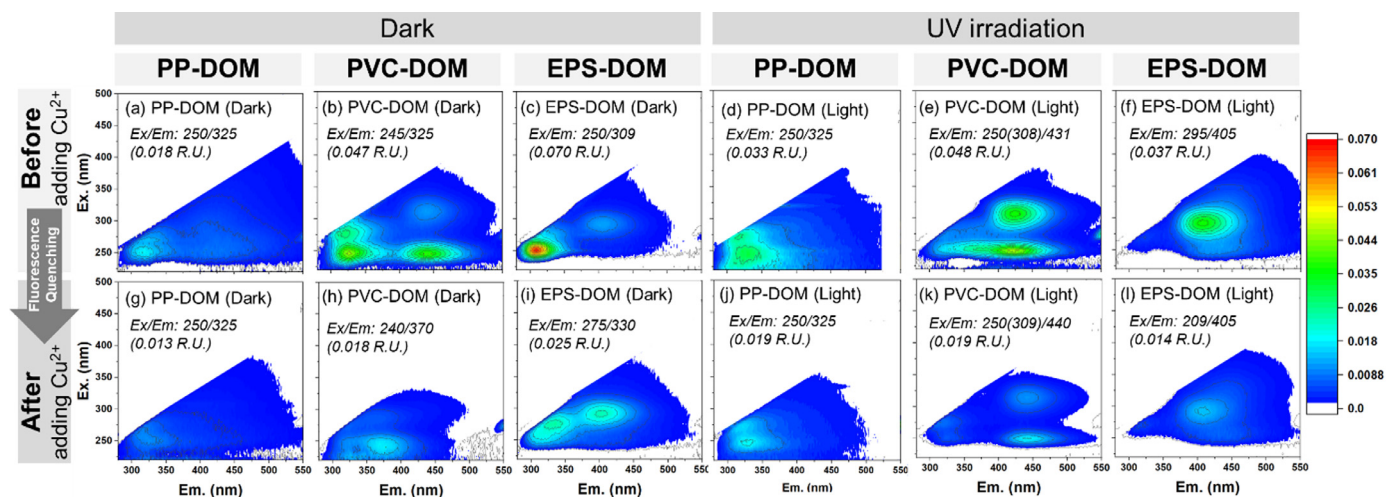


Fig. 2. Fluorescence EEM plots of the DOM leached from (a and g) PP, (b and h) PVC, and (c and i) EPS in the dark, and from (d and j) PP, (e and k) PVC and (f and l) EPS under UV irradiation conditions after 14 days of leaching (5 g-MP/L) (a to f) before or (g to l) after the addition of copper (200 $\mu\text{mol/L}$). The numbers in each figure indicate the position (Ex/Em) of the strongest peak in the EEM and its intensity.

the current situation, in which many soil/sediment environments are polluted with PVC plastics (Van Cauwenberghe et al., 2015; Wang et al., 2019). Thus, it is expected that a substantial amount of DOM could be leached from PVC in such environments. In addition, large differences in the piece number-normalized DOC concentrations of MP-DOM were found between the two different leaching conditions (Fig. 1e).

3.1.3. Fluorescence EEMs

The fluorescence EEMs of the MP-DOM samples are shown in Fig. 2. The samples were obtained from the leaching solutions at 5 g-MP/L. As all samples were diluted to the same DOC concentration (i.e., 0.25 mg-C/L), they were comparable to one another on the same scale. No fluorescence peak was detected for the control sample (i.e., the artificial freshwater solution without MPs) (Fig. S2a), which indicated that the observed fluorescence peaks originated solely from the plastics added to the artificial freshwater solution.

Regardless of the plastic type, prominent peaks appeared in the phenol/protein-like fluorescence region, which are typically defined as peak B (~225(-280)/~305 nm) and peak T (~225(-280)/~350 nm) (Ex/Em) (Coble, 1996) of the EEM for the dark-treated MP-DOM (Figs. 2a–c). The peak B may represent phenol-like substances (Carstea et al., 2016; Ou et al., 2014), while the peak T is typically related to bio-labile properties, its presence in the EEMs is in line with a previous study, which reported that a substantial portion (approximately 60%) of the DOM leached from plastics was degraded in less than 5 days under microbial incubation (Romera-Castillo et al., 2018). The dark-treated MP-DOM samples exhibited additional peaks in the humic-like fluorescence region, from 260 to 310 nm (Ex) and 405 nm (Em). Except for PP, the humic-like fluorescence was more pronounced for the UV-irradiated samples, suggesting that the fluorescence might be associated with photo-induced structures (Figs. 2d and f). For example, the humic-like peak intensity at 295/405 nm (Ex/Em) was higher for the EPS-DOM obtained under UV irradiation (0.037 R.U.) compared to that in the dark (0.011 R.U.). In contrast, the phenol/protein-like peak at 250/309 nm (Ex/Em) showed a lower intensity for the irradiated MP-DOM than the dark-treated counterparts (e.g., 0.070 versus 0.001 R.U. for EPS-DOM), which can be attributed to photolytic degradation. The photo-labile property of protein-like fluorophores has been previously reported for aquatic NOM (Phong and Hur, 2015).

Changes in the EEM spectra upon the addition of copper were compared for three different plastic types under dark and UV irradiation conditions (Fig. 2a–f versus 2g to 2l). Fluorescence quenching by copper addition was observed for all MP-DOM similarly to the NOM samples, which suggested that electronic structural changes occurred in MP-DOM via the formation of complexes with copper (Plaza et al., 2006). However, the quenching behavior was not the same for all MP-DOM samples, indicating that the degree of quenching and the associated structures may depend upon the plastic type and the leaching conditions. EEM alone is not capable of characterizing the interactions of independent fluorophores with copper as the apparent EEM peaks may consist of multiple fluorescent components. Thus, it is necessary to track fluorescence quenching of independent fluorescent components identified from EEM-PARAFAC.

3.2. Copper-binding characteristics of different fluorescent components

3.2.1. Fluorescent components identified by PARAFAC modeling

The PARAFAC modeling revealed that the three-component model best describes the copper-inducing variations in the fluorescence features of the MP-DOM samples with the core consistency of 95.3% (Fig. 3 and Table S3). Component 1 (C1) peaked at 265(325)/463 nm (Ex/Em). Components 2 (C2) and 3 (C3) exhibited maxima at 250(325)/324 nm (Ex/Em) and 295(250)/411 nm (Ex/Em), respectively. The peak locations of C2 and C3 were consistent with those of the previous EEM spectra of the MP-DOM under dark and UV irradiation conditions. These fluorescent components are analogous to those typically found in natural aquatic systems (Brogi et al., 2020; Kothawala et al., 2014) as well as those obtained from the leaching of plastic materials (Lee et al., 2020b) (Table S3). C1 can be assigned to a terrestrial humic-like component, which roughly represents the fluorescence feature of the NOM materials used in this study.

3.2.2. Fluorescence quenching behavior of different fluorescent components

The quenching trend of each FDOM component upon the addition of copper is shown in Fig. S3. For the same plastic type, the quenching curves differed greatly depending on the FDOM component, the plastic types (i.e., PP, PVC, and EPS), and the leaching conditions (i.e., dark and UV irradiation). In the dark-treated MP-DOM, the two plastic-derived components, C2 and C3,

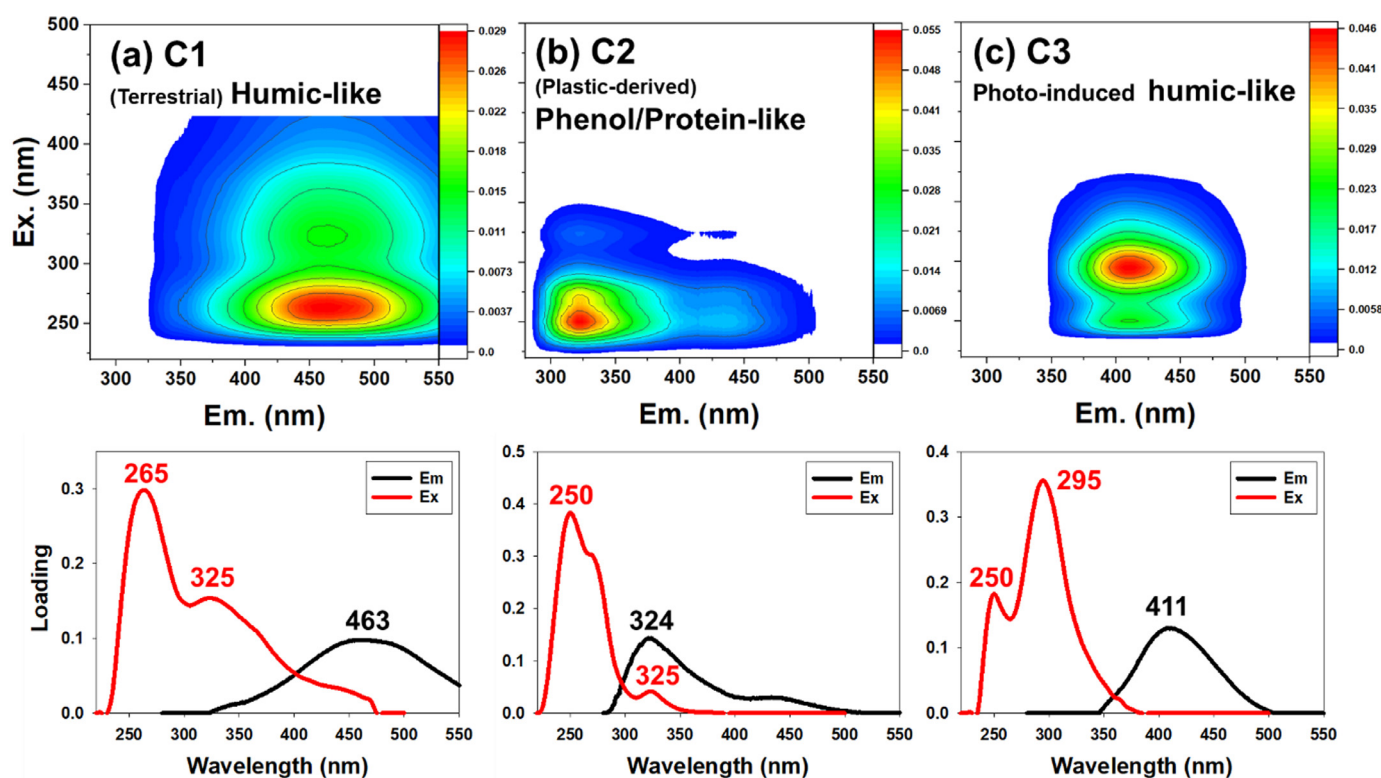


Fig. 3. PARAFAC model output showing three different fluorescent components (up) and the corresponding excitation/emission loadings (down).

showed obvious fluorescence quenching upon the addition of copper, while negligible quenching was observed for C1 (Fig. S3). Even the same FDOM component showed different degrees of fluorescence quenching, depending on the plastic type (Fig. S3). For example, for the dark-treated MP-DOM, the extent of quenching in phenol/protein-like C2 reached a reduction of up to $48.6 \pm 3.6\%$ for EPS and $48.3 \pm 2.7\%$ for PVC, while it was only $28.5 \pm 1.2\%$ for PP. However, the extent of quenching of the PP-DOM, in which no humic-like fluorescence peak was shown, was more pronounced under UV-irradiation versus dark conditions (reduction of up to $68.9 \pm 2.7\%$ for C2). The metal addition-induced quenching for the phenol/protein-like component in DOM has been previously reported in many studies (Hu et al., 2017; Hur and Lee, 2011). This result strongly implies that the phenol/protein-like component contains structures that are actively involved in copper binding, irrespective of the plastic type. On the other hand, the extent of quenching in the plastic-derived humic component (C3) was more pronounced for the PVC-DOM and EPS-DOM under UV irradiation than under dark conditions (EPS-DOM: $69.2 \pm 7.8\%$ under UV irradiation versus $61.0 \pm 1.4\%$ in the dark; PVC-DOM: $67.7 \pm 0.1\%$ versus $54.4 \pm 4.3\%$) (Fig. S3). The greater extent of fluorescence quenching of the humic-like component in the irradiated MP-DOM may be associated with the presence of more acidic functional groups in the MP-DOM obtained under UV irradiation than under dark conditions. This explanation is supported by a previous study that used mass spectroscopy, in which oxygen-containing groups such as carboxylate were detected in the leached solution from UV-irradiated plastics (Gewert et al., 2018). In the same context, previous studies using NOM have shown that aromatic structures and acidic functional groups are responsible for strong copper binding (Plaza et al., 2006). Slight increase and/or fluctuation of some components in the quenching curves (Fig. S3) can be ascribed to the changes of quantum yields as a result of structural modification of fluorescent molecules caused by high levels of copper (Yamashita and Jaffé, 2008).

NOM samples (i.e., SRFA and ESHA) showed clear fluorescence quenching in C1 but negligible quenching in C2 and C3. The maximum extent of C1 quenching was $44.7 \pm 0.6\%$ for SRFA and $83.7 \pm 0.4\%$ for ESHA. Interestingly, C2 was clearly quenched by copper addition to MP-DOM, but not for the NOM samples. This result suggests that the C2 component may have completely different structures between MP-DOM and NOM in terms of copper binding, even though it has identical spectral features.

3.2.3. Comparison of copper-binding parameters for different fluorescent components

To explore differences in the binding properties of different fluorescent components and different MP-DOM samples, the copper-binding parameters were calculated using the best-fit of the modified Stern-Volmer equation based on the F_{max} values of the individual components exhibiting quenching behaviors (Table 1 and Fig. 4). The fluorescent components included in the model fittings were C1 from SRFA and ESHA, C2 in the MP-DOM samples from PP, PVC, EPS in the dark and PP obtained under UV-irradiation, and C3 from EPS-DOM and PVC-DOM obtained under both dark and UV irradiation conditions. The results for the copper-binding parameter of the fluorescent components are listed in Table 1 with statistical significance ($p < 0.01$).

A range of binding constants (or stability constants) was observed for the same fluorescent component among the different MP-DOM samples (Table 1). For example, the $\log K_M$ values of the C2 component in the dark-treated MP-DOM samples ranged from 1.05 ± 0.01 to 3.09 ± 0.08 , with variations depending on the plastic type. Independent of the plastic type and the fluorescent component, the UV-irradiated MP-DOM exhibited higher stability constants than the dark-treated counterparts, as shown by the $\log K_M$ values of C3 ranging from 4.82 ± 0.72 to 5.36 ± 0.77 for the former versus from 1.97 ± 0.03 to 3.60 ± 0.05 for the latter (Table 1). For the PP-DOM, the $\log K_M$ values of C2 were 4.08 ± 0.25 and 2.62 ± 0.09 for UV-irradiation and dark conditions, respectively.

Table 1
Copper-binding parameters of three different fluorescent components calculated by the modified Stern–Volmer equation using the representative NOM and MP-DOM samples under different leaching conditions.

	Conditions	Type	PARAFAC Components †	Modified Stern–Volmer		
				r^a	$\log K_M^b$	f^c
MP-DOM	Dark	EPS	C2	0.993 *	1.05 ±0.01	0.81 ±0.01
			C3	0.977 *	3.60 ±0.04	0.46 ±0.07
		PVC	C2	0.932 *	3.09 ±0.08	0.63 ±0.05
			C3	0.985 *	1.97 ±0.03	0.47 ±0.02
		PP	C2	0.984 *	2.62 ±0.09	0.36 ±0.06
MP-DOM	UV irradiation	EPS	C3	0.994 *	5.36 ±0.77	0.51 ±0.06
			C3	0.985 *	4.82 ±0.72	0.46 ±0.02
		PVC	C3	0.952 *	4.08 ±0.25	0.61 ±0.05
			C2	0.982 *	5.21 ±0.73	0.37 ±0.04
		PP	C2	0.989 *	5.56 ±0.74	0.46 ±0.02
NOM		SRFA	C1	0.982 *	5.21 ±0.73	0.37 ±0.04
		ESHA	C1	0.989 *	5.56 ±0.74	0.46 ±0.02

† The quenched components were selected based on the observed changes in the F_{max} values of the individual fluorescence components with increasing copper concentrations (5 to 200 $\mu\text{mol/L}$) in Figure S1.

* $p < 0.01$.

^a Correlation coefficients (r) between predicted and observed fluorescence intensity.

^b Conditional stability constants ($\log K_M$).

^c Fraction of the initial fluorescence corresponding to the binding sites (f).

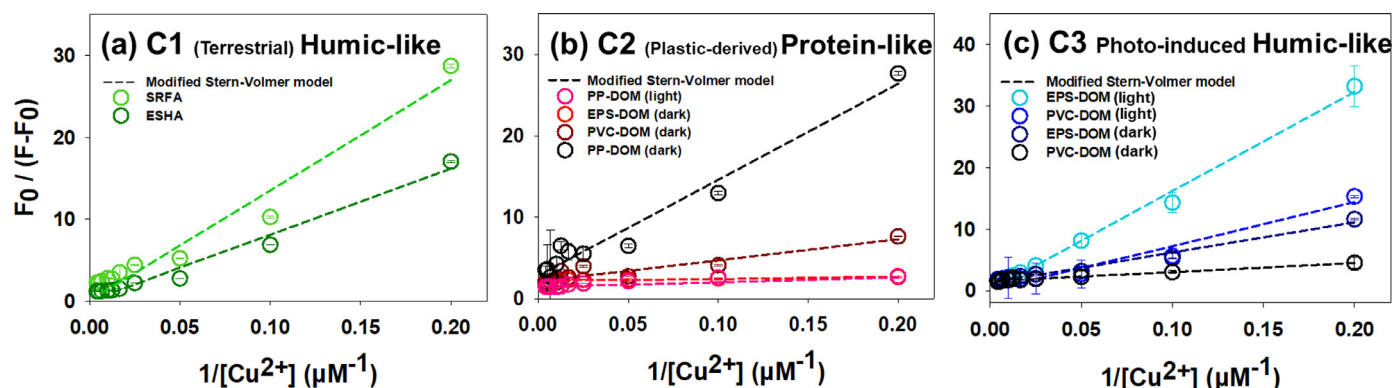


Fig. 4. Modified Stern–Volmer plots of the fluorescence quenching of three individual fluorescent components of SRFA and ESHA as representative NOM and the plastic-derived DOM under dark and UV irradiation conditions. The quenched components (a: C1 for SRFA and ESHA; b: C2 for PP-DOM, PVC-DOM, EPS-DOM in the dark and PP-DOM under UV irradiation condition; c: C3 for PVC-DOM and EPS-DOM under dark and UV irradiation conditions) were selected based on the observed changes (i.e., consistent reduction) in the F_{max} values of the components with increasing copper concentrations (from 5 to 200 $\mu\text{mol/L}$) in Figure S1.

This result can be ascribed to the previous observation regarding the presence of oxygen-containing functional groups in irradiated MP-DOM.

Interestingly, the calculated stability constants of the C3 component in the MP-DOM samples were comparable to or even greater than those of similar fluorescence peaks previously reported for aquatic/terrestrial NOM (ranging from 3.97 to 5.39) (Hur and Lee, 2011; Lee and Hur, 2017; Xu et al., 2013a, 2013b). For the NOM samples in the present study, the humic-like component (C1) exhibited significant model parameters, and the stability constants were similar to those of C3 in the irradiated MP-DOM (Table 1). These results suggest that dissolved organic substances from the photochemical breakdown of plastics can interact with metals strongly enough to alter the fate and transport of metals in natural and engineered systems, which can be comparable to the effect of NOM on metal transport. In contrast to the stability constants, there was no consistent trend of the f values between the irradiated and the dark-treated samples (Table 1). However, the

photo-induced humic-like component (C3) exhibited lower f values compared to phenol/protein-like C2 for both EPS- and PVC-DOM. The results suggested that the fraction of the participating binding sites might be more affected by variations in FDOM components than the leaching conditions for MP-DOM.

In fact, interaction of metals with the surface of MP particles has also been studied in recent years (Guan et al., 2020; Turner and Holmes, 2015). In the studies, it was found that biofilm development on MP surfaces could enhance the metal adsorption via alteration of the physical and chemical properties of the MPs' surfaces in a way to enrich carboxyl, amino, and phenyl-OH groups (Guan et al., 2020). However, regardless of the biofilm formation, MP particles exhibited a much lower adsorption tendency than natural particles such as suspended sediment (Guan et al., 2020). The result of the previous study is in stark contrast to the comparable copper binding affinity of MP-DOM (especially, irradiated MP-DOM) to those of NOM in this study (Table 1).

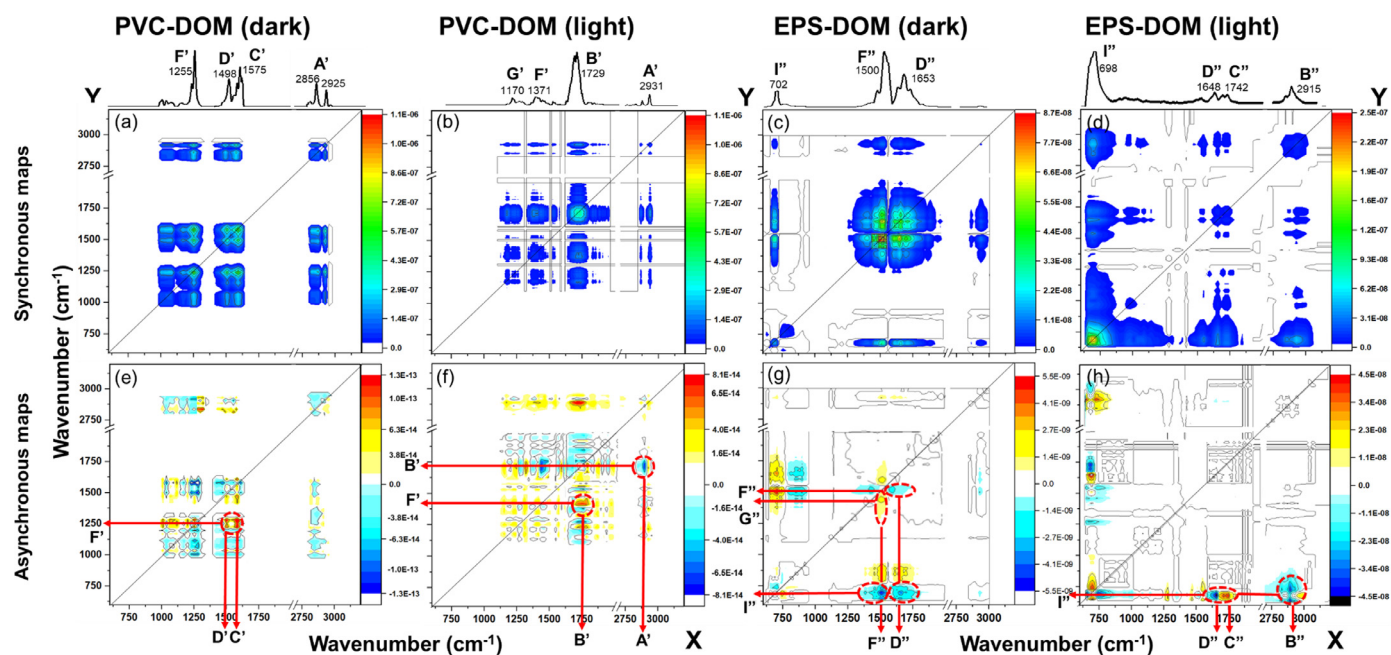


Fig. 5. (a to d) Synchronous and (e to h) asynchronous maps of 2D-COS using the FTIR spectra at 1000–3100 cm^{-1} . The DOM leached from (a, b, e, and f) PVC and (c, d, g, and h) EPS with increasing copper concentrations under (a, c, e, and g) dark and (b, d, f, and h) UV irradiation conditions. The IR spectra on the diagonal of the synchronous map are displayed above the maps. The red lines and the corresponding letters indicate the main peaks of the asynchronous maps. The signs of the main peaks are shown in Tables S4 and S5.

3.3. Change in FTIR spectra with copper addition: 2D-CoIR analysis

To obtain further information regarding the sequential changes in the functional groups of MP-DOM with the addition of copper, 2D-COS was performed with a series of FTIR spectra obtained with varying amounts of added copper. To examine the effect of the leaching conditions on changes in the FTIR spectra, the 2D-COS was explored only for PVC- and EPS-DOM. Regardless of the plastic type and the leaching conditions, all FTIR peaks identified in the original MP-DOM samples were observed after the addition of copper with varying intensities. The spectral changes on copper addition are presented in Fig. S4. The extent of changes in the peak intensities differed depending on the peak locations and sample types (Fig. S4).

On the diagonal lines of the synchronous maps (Figs. 5a–d), several distinctive peaks were observed, including peaks A', C', D', and F' for the dark-treated PVC-DOM, peaks D'', F'', and I'' for the dark-treated EPS-DOM, peaks A', B', F', and G' for the irradiated PVC-DOM, and peaks B'', C'', D'', and I'' for the irradiated EPS-DOM. The signs of the cross-peaks were positive in all synchronous maps, indicating that the spectral changes associated with copper binding occurred in the same direction. In addition, the asynchronous map revealed information concerning the sequential changes in the FTIR spectra in response to increasing copper concentrations. For the dark-treated PVC-DOM, two positive signed peaks were identified at the locations (x-axis/y-axis) of peaks C'/F' and D'/F'. The peak locations corresponded to the same positive region in the synchronous map (Figs. 5e–h and Table S4). According to Noda's rules (Hur and Lee, 2011; Noda et al., 2000), the features can be interpreted as the binding affinity for copper increasing of carboxylates in additives (peak C') > bisphenol A(BPA) (peak D') > CH bends (peak F'). Under the same rules, the sequential changes of the dark-treated EPS-DOM occurred in the order of aromatic CH (peak I'') > aromatic ring (peak F'') > C = C (peak D'') > CH₂ bend (peak G'). These results suggest that leached additives from plastic have stronger binding affinities for copper than other leached structures, and that aromatic ring structures of plastics are more

active in binding copper than the common plastic structures related to CH₂ bend.

For the irradiated MP-DOM, one positively and one negatively signed cross-peaks were found in the asynchronous map of the PVC-DOM at the x/y locations corresponding to peaks B'/F' and A'/B', respectively. For the irradiated EPS-DOM, there was one positively signed peak at C''/I'' and two negatively signed cross-peaks at B''/I'' and D''/I''. According to Noda's rules, the features can lead to the following sequential orders of peak B' (C = O) > F' (CH bend) > A' (CH stretch) for PVC-DOM, and peak C'' (C = O) > I'' (aromatic CH) > D'' (C = C) > B'' (CH stretch) for EPS-DOM. From the results, the oxidized structures of MP-DOM revealed their priority in the sequence of copper binding over the additives and polymer-derived substances irrespective of the plastic type. The general trend of the binding preferences in different functional groups agrees with those previously reported for NOM. For example, oxygen-containing structures of NOM such as carboxylic group have revealed a stronger binding affinity for copper compared to other functional groups based on the same analytic method (Chen et al., 2015; Hu et al., 2019; Huang et al., 2018). Furthermore, from the perspective of the environmental reactivity of MP-DOM, it is worth noting a recent study demonstrated stronger interaction of oxidized structures in irradiated MP-DOM with mineral surfaces, which was also revealed by utilizing 2D-COS based on FTIR spectra (Lee and Hur, 2020).

3.4. Environmental implications and future studies

This study demonstrated the capability of plastic-derived DOM to bind copper via the FQM. A range of binding constants were found among the different fluorescent components identified within the bulk MP-DOM samples. 2D-COS combined with FTIR spectra provided further insights into the heterogeneous distribution of copper-binding sites within bulk MP-DOM as well as the sequence in sites with higher affinity. Considering the massive production of plastics that might result in a substantial amount of MP-DOM released into natural ecosystems, this information is essential

for understanding the fate and transport of metals in MP-polluted environments. The environmental fate of metals might be altered by interacting with the previously overlooked MP-DOM under such circumstances, and the information on metal binding with NOM alone may be misleading to fully understand the fate and transport of metals in such environments. For example, there might be competition between NOM and MP-DOM for binding metals in MP-polluted environments. As this study used copper as a model metal, further metal-binding experiments using other trace metals are recommended to extend and generalize the findings of this work.

The extent of the interaction can be strongly affected by several factors such as leaching conditions, plastic types, and amounts of additives contained in MPs. The presented results demonstrated that the interactions between copper and plastic-derived DOM, especially irradiated MP-DOM, could be as strong as those with NOM. Thus, a tool to distinguish between naturally occurring and plastic-derived DOM in natural environments is required to properly identify the environmental impacts (e.g., interactions with metals) of plastic-derived DOM because of its similar environmental behavior as NOM. For example, although the C3 revealed a distinctive for the MP-DOM produced under UV-irradiation in this study, this fluorescence feature overlapped with those from common aquatic NOM, hampering the clear distinction of DOM with MP origins from those that originate naturally.

4. Conclusions

This is the first report to demonstrate the metal-binding ability of plastic-derived DOM. The following conclusions can be drawn from the results of this study.

- (1) This study demonstrated the interactions between plastic-derived DOM and copper via the FQM. The EEM-PARAFAC identified two specific fluorescent components from MP-DOM leached under dark and UV irradiation conditions. The two plastic-derived components (phenol/protein-like C2 and photo-induced humic-like C3) showed clear fluorescence quenching behaviors with increasing copper concentrations.
- (2) MP-DOM exhibited a high binding affinity towards copper. For EPS and PVC plastics, the stability constants, or $\log K_M$, were higher for the UV-irradiated than the dark-treated MP-DOM. The results highlight the impact of the leaching conditions on the metal-binding behavior of MP-DOM.
- (3) 2D-COS combined with FTIR revealed preferential binding affinities for copper among different functional groups in MP-DOM. Additives and aromatic ring structures in MP-DOM interacted with copper more strongly than polymer-associated structures in the dark-treated MP-DOM, whereas oxygen-containing functional groups were found to be the most preferred structures for copper binding among all the structures identified from the FTIR of the UV-irradiated MP-DOM.
- (4) The estimated binding constants of MP-DOM were comparable to those of the aquatic/terrestrial NOM. This finding implies that the interaction of plastic-derived DOM with trace metals should be taken into account to fully understand the fate and consequences of metals in MP-polluted environments.

Declaration of Competing Interest

The authors declare that they have no known competing financial interests or personal relationships that could have appeared to influence the work reported in this paper.

Acknowledgements

This work was supported by grants from the National Research Foundation of Korea (NRF) funded by the Korean government (2020R1A2C2007248 and 2020R1A4A2002823).

Supplementary materials

Supplementary material associated with this article can be found, in the online version, at doi:10.1016/j.watres.2020.116775.

References

- Alimi, O.S., Farnier Budarz, J., Hernandez, L.M., Tufenkji, N., 2018. Microplastics and nanoplastics in aquatic environments: aggregation, deposition, and enhanced contaminant transport. *Environ. Sci. Technol.* 52 (4), 1704–1724.
- Broggi, S.R., Balestra, C., Casotti, R., Cossarini, G., Galletti, Y., Gonnelli, M., Vestri, S., Santinelli, C., 2020. Time resolved data unveils the complex DOM dynamics in a Mediterranean river. *Sci. Total Environ.*, 139212.
- Carstea, E.M., Bridgeman, J., Baker, A., Reynolds, D.M., 2016. Fluorescence spectroscopy for wastewater monitoring: a review. *Water Res.* 95, 205–219.
- Chae, Y., An, Y.-J., 2018. Current research trends on plastic pollution and ecological impacts on the soil ecosystem: a review. *Environ. Pollut.* 240, 387–395.
- Chen, W., Habibul, N., Liu, X.-Y., Sheng, G.-P., Yu, H.-Q., 2015. FTIR and synchronous fluorescence heterospectral two-dimensional correlation analyses on the binding characteristics of copper onto dissolved organic matter. *Environ. Sci. Technol.* 49 (4), 2052–2058.
- Chen, W., Ouyang, Z.-Y., Qian, C., Yu, H.-Q., 2018. Induced structural changes of humic acid by exposure of polystyrene microplastics: a spectroscopic insight. *Environ. Pollut.* 233, 1–7.
- Coble, P.G., 1996. Characterization of marine and terrestrial DOM in seawater using excitation-emission matrix spectroscopy. *Mar. Chem.* 51 (4), 325–346.
- Croué, J.-P., Benedetti, M., Violleau, D., Leenheer, J., 2003. Characterization and copper binding of humic and nonhumic organic matter isolated from the South Platte river: evidence for the presence of nitrogenous binding site. *Environ. Sci. Technol.* 37 (2), 328–336.
- da Silva, J.C.E., Machado, A.A., Oliveira, C.J., Pinto, M.S., 1998. Fluorescence quenching of anthropogenic fulvic acids by Cu (II), Fe (III) and UO₂²⁺. *Talanta* 45 (6), 1155–1165.
- de Polo, A., Scrimshaw, M.D., 2012. Challenges for the development of a biotic ligand model predicting copper toxicity in estuaries and seas. *Environ. Toxicol. Chem.* 31 (2), 230–238.
- Eerkes-Medrano, D., Thompson, R.C., Aldridge, D.C., 2015. Microplastics in freshwater systems: a review of the emerging threats, identification of knowledge gaps and prioritisation of research needs. *Water Res.* 75, 63–82.
- Galgani, L., Engel, A., Rossi, C., Donati, A., Loisel, S.A., 2018. Polystyrene microplastics increase microbial release of marine Chromophoric Dissolved Organic Matter in microcosm experiments. *Sci. Rep.* 8 (1), 14635.
- Gardette, M., Perthue, A., Gardette, J.-L., Janeska, T., Földes, E., Pukánszky, B., Therias, S., 2013. Photo-and thermal-oxidation of polyethylene: comparison of mechanisms and influence of unsaturation content. *Polym. Degrad. Stabil.* 98 (11), 2383–2390.
- Gewert, B., Plassmann, M., Sandblom, O., MacLeod, M., 2018. Identification of chain scission products released to water by plastic exposed to ultraviolet light. *Environ. Sci. Technol. Lett.* 5 (5), 272–276.
- Guan, J., Qi, K., Wang, J., Wang, W., Wang, Z., Lu, N., Qu, J., 2020. Microplastics as an emerging anthropogenic vector of trace metals in freshwater: significance of biofilms and comparison with natural substrates. *Water Res.* 184, 116205.
- Gugumus, F., 1999. Formation of ester functional groups in oxidizing polymers. *Polym. Degrad. Stabil.* 65 (1), 5–13.
- Guo, X.-J., He, X.-S., Li, C.-W., Li, N.-X., 2019. The binding properties of copper and lead onto compost-derived DOM using Fourier-transform infrared, UV–vis and fluorescence spectra combined with two-dimensional correlation analysis. *J. Hazard. Mater.* 365, 457–466.
- Hays, M.D., Ryan, D.K., Pennell, S., 2004. A modified multisite Stern–Volmer equation for the determination of conditional stability constants and ligand concentrations of soil fulvic acid with metal ions. *Anal. Chem.* 76 (3), 848–854.
- He, D., Luo, Y., Lu, S., Liu, M., Song, Y., Lei, L., 2018. Microplastics in soils: analytical methods, pollution characteristics and ecological risks. *Trac-Trend Anal. Chem.* 109, 163–172.
- Hermabessiere, L., Dehaut, A., Paul-Pont, I., Lacroix, C., Jezequel, R., Soudant, P., Duflos, G., 2017. Occurrence and effects of plastic additives on marine environments and organisms: a review. *Chemosphere* 182, 781–793.
- Hu, B., Wang, P., Wang, C., Qian, J., Bao, T., Shi, Y., 2019. Investigating spectroscopic and copper-binding characteristics of organic matter derived from sediments and suspended particles using EEM-PARAFAC combined with two-dimensional fluorescence/FTIR correlation analyses. *Chemosphere* 219, 45–53.
- Hu, B., Wang, P., Wang, C., Qian, J., Hou, J., Cui, X., Zhang, N., 2017. The effect of anthropogenic impoundment on dissolved organic matter characteristics and copper binding affinity: insights from fluorescence spectroscopy. *Chemosphere* 188, 424–433.
- Huang, M., Li, Z., Huang, B., Luo, N., Zhang, Q., Zhai, X., Zeng, G., 2018. Investigating binding characteristics of cadmium and copper to DOM derived from compost

- and rice straw using EEM-PARAFAC combined with two-dimensional FTIR correlation analyses. *J. Hazard. Mater.* 344, 539–548.
- Hur, J., Lee, B.-M., 2011. Characterization of binding site heterogeneity for copper within dissolved organic matter fractions using two-dimensional correlation fluorescence spectroscopy. *Chemosphere* 83 (11), 1603–1611.
- Jang, M., Shim, W.J., Han, G.M., Rani, M., Song, Y.K., Hong, S.H., 2017. Widespread detection of a brominated flame retardant, hexabromocyclododecane, in expanded polystyrene marine debris and microplastics from South Korea and the Asia-Pacific coastal region. *Environ. Pollut.* 231, 785–794.
- Jung, M.R., Horgen, F.D., Orski, S.V., Rodriguez, V., Beers, K.L., Balazs, G.H., Jones, T.T., Work, T.M., Brignac, K.C., Royer, S.-J., 2018. Validation of ATR FT-IR to identify polymers of plastic marine debris, including those ingested by marine organisms. *Mar. Pollut. Bull.* 127, 704–716.
- Kothawala, D.N., Stedmon, C.A., Müller, R.A., Weyhenmeyer, G.A., Köhler, S.J., Tranvik, L.J., 2014. Controls of dissolved organic matter quality: evidence from a large-scale boreal lake survey. *Glob. Change Biol.* 20 (4), 1101–1114.
- Lawaetz, A.J., Stedmon, C.A., 2009. Fluorescence intensity calibration using the Raman scatter peak of water. *Appl. Spectrosc.* 63 (8), 936–940.
- Lee, M.-H., Han, S.-J., Lee, Y.K., Ike, I.A., Ok, Y.S., Hur, J., 2020a. Enhancing copper binding property of compost-derived humic substances by biochar amendment: further insight from two-dimensional correlation spectroscopy. *J. Hazard. Mater.* 390, 121128.
- Lee, Y.-K., Hur, J., 2017. Using two-dimensional correlation size exclusion chromatography (2D-CoSEC) to explore the size-dependent heterogeneity of humic substances for copper binding. *Environ. Pollut.* 227, 490–497.
- Lee, Y.K., Hur, J., 2020. Adsorption of microplastic-derived organic matter onto minerals. *Water Res.*, 116426.
- Lee, Y.K., Murphy, K., Hur, J., 2020b. Fluorescence signatures of dissolved organic matter leached from microplastics: polymers and additives. *Environ. Sci. Technol.*
- Lee, Y.K., Romera-Castillo, C., Hong, S., Hur, J., 2020c. Characteristics of microplastic polymer-derived dissolved organic matter and its potential as a disinfection byproduct precursor. *Water Res.*, 115678.
- Li, W., Zhang, F., Ye, Q., Wu, D., Wang, L., Yu, Y., Deng, B., Du, J., 2017. Composition and copper binding properties of aquatic fulvic acids in eutrophic Taihu Lake, China. *Chemosph.* 172, 496–504.
- Lucki, J., Rånby, B., 1979. Photo-oxidation of polystyrene—Part 2: formation of carbonyl groups in photo-oxidised polystyrene. *Polym. Degrad. Stabil.* 1 (3), 165–179.
- Majedi, S.M., Kelly, B.C., Lee, H.K., 2014. Combined effects of water temperature and chemistry on the environmental fate and behavior of nanosized zinc oxide. *Sci. Total Environ.* 496, 585–593.
- Murphy, K.R., Stedmon, C.A., Graeber, D., Bro, R., 2013. Fluorescence spectroscopy and multi-way techniques. *PARAFAC. Anal. Methods* 5 (23), 6557–6566.
- Noda, I., 2016. Techniques useful in two-dimensional correlation and codistribution spectroscopy (2DCOS and 2DCDS) analyses. *J. Mol. Struct.* 1124, 29–41.
- Noda, I., Dowrey, A., Haynes, J., Marcott, C., 2007. *Phys. Prop. Polym.*, pp. 395–406 Springer.
- Noda, I., Dowrey, A., Marcott, C., Story, G., Ozaki, Y., 2000. Generalized two-dimensional correlation spectroscopy. *Appl. Spectrosc.* 54 (7), 236A–248A.
- Noda, I., Ozaki, Y., 2005. *Two-dimensional Correlation Spectroscopy: Applications in Vibrational and Optical Spectroscopy.* John Wiley & Sons.
- Ou, H.-S., Wei, C.-H., Mo, C.-H., Wu, H.-Z., Ren, Y. and Feng, C.-H.J.C. 2014. Novel insights into anoxic/aerobic1/aerobic2 biological fluidized-bed system for coke wastewater treatment by fluorescence excitation–emission matrix spectra coupled with parallel factor analysis. 113, 158–164.
- Park, Y., Noda, I., Jung, Y.M., 2016. Novel developments and applications of two-dimensional correlation spectroscopy. *J. Mol. Struct.* 1124, 11–28.
- Phong, D.D., Hur, J., 2015. Insight into photocatalytic degradation of dissolved organic matter in UVA/TiO₂ systems revealed by fluorescence EEM-PARAFAC. *Water Res.* 87, 119–126.
- Plaza, C., Brunetti, G., Senesi, N., Polo, A., 2006. Molecular and quantitative analysis of metal ion binding to humic acids from sewage sludge and sludge-amended soils by fluorescence spectroscopy. *Environ. Sci. Technol.* 40 (3), 917–923.
- Potthoff, A., Oelschlägel, K., Schmitt-Jansen, M., Rummel, C.D., Kühnel, D., 2017. From the sea to the laboratory: characterization of microplastic as prerequisite for the assessment of ecotoxicological impact. *Integr. Environ. Assess.* 13 (3), 500–504.
- Romera-Castillo, C., Pinto, M., Langer, T.M., Álvarez-Salgado, X.A., Herndl, G.J., 2018. Dissolved organic carbon leaching from plastics stimulates microbial activity in the ocean. *Nat. Commun.* 9 (1), 1430.
- Ryan, D.K., Weber, J.H., 1982. Fluorescence quenching titration for determination of complexing capacities and stability constants of fulvic acid. *Anal. Chem.* 54 (6), 986–990.
- Santore, R.C., Di Toro, D.M., Paquin, P.R., Allen, H.E., Meyer, J.S., 2001. Biotic ligand model of the acute toxicity of metals. 2. Application to acute copper toxicity in freshwater fish and *Daphnia*. *Environ. Toxicol. Chem.* 20 (10), 2397–2402.
- Shi, Z., Wang, P., Peng, L., Lin, Z., Dang, Z., 2016. Kinetics of heavy metal dissociation from natural organic matter: roles of the carboxylic and phenolic sites. *Environ. Sci. Technol.* 50 (19), 10476–10484.
- Song, F., Wu, F., Guo, F., Wang, H., Feng, W., Zhou, M., Deng, Y., Bai, Y., Xing, B., Giesy, J.P., 2017a. Interactions between stepwise-eluted sub-fractions of fulvic acids and protons revealed by fluorescence titration combined with EEM-PARAFAC. *Sci. Total Environ.* 605, 58–65.
- Song, Y.K., Hong, S.H., Jang, M., Han, G.M., Jung, S.W., Shim, W.J., 2017b. Combined effects of UV exposure duration and mechanical abrasion on microplastic fragmentation by polymer type. *Environ. Sci. Technol.* 51 (8), 4368–4376.
- Suhrhoff, T.J., Scholz-Böttcher, B.M., 2016. Qualitative impact of salinity, UV radiation and turbulence on leaching of organic plastic additives from four common plastics—a lab experiment. *Mar. Pollut. Bull.* 102 (1), 84–94.
- Syberg, K., Khan, F.R., Selck, H., Palmqvist, A., Banta, G.T., Daley, J., Sano, L., Duhaime, M.B., 2015. Microplastics: addressing ecological risk through lessons learned. *Environ. Toxicol. Chem.* 34 (5), 945–953.
- Turner, A., Holmes, L.A., 2015. Adsorption of trace metals by microplastic pellets in fresh water. *Environ. Chem.* 12 (5), 600–610.
- Van Cauwenberghe, L., Devriese, L., Galgani, F., Robbins, J., Janssen, C.R., 2015. Microplastics in sediments: a review of techniques, occurrence and effects. *Mar. Environ. Res.* 111, 5–17.
- Verleye, G.A., Roeges, N.P., De Moor, M.O., 2001. *Easy Identification of Plastics and Rubbers.* iSmithers Rapra Publishing.
- Wang, J., Liu, X., Li, Y., Powell, T., Wang, X., Wang, G., Zhang, P., 2019. Microplastics as contaminants in the soil environment: a mini-review. *Sci. Total Environ.* 691, 848–857.
- Wang, Z., Cao, J., Meng, F., 2015. Interactions between protein-like and humic-like components in dissolved organic matter revealed by fluorescence quenching. *Water Res.* 68, 404–413.
- Wu, F., Cai, Y., Evans, D., Dillon, P., 2004. Complexation between Hg (II) and dissolved organic matter in stream waters: an application of fluorescence spectroscopy. *Biogeochemistry* 71 (3), 339–351.
- Xu, H., Yan, Z., Cai, H., Yu, G., Yang, L., Jiang, H., 2013a. Heterogeneity in metal binding by individual fluorescent components in a eutrophic algae-rich lake. *Ecotoxicol. Environ. Saf.* 98, 266–272.
- Xu, H., Yu, G., Yang, L., Jiang, H., 2013b. Combination of two-dimensional correlation spectroscopy and parallel factor analysis to characterize the binding of heavy metals with DOM in lake sediments. *J. Hazard. Mater.* 263, 412–421.
- Yamashita, Y., Jaffé, R., 2008. Characterizing the interactions between trace metals and dissolved organic matter using excitation–emission matrix and parallel factor analysis. *Environ. Sci. Technol.* 42 (19), 7374–7379.
- Yang, L., Han, D.H., Lee, B.-M., Hur, J., 2015. Characterizing treated wastewaters of different industries using clustered fluorescence EEM-PARAFAC and FT-IR spectroscopy: implications for downstream impact and source identification. *Chemosphere* 127, 222–228.

Supporting Information:

Water Research

Copper-binding properties of microplastic-derived dissolved organic matter revealed by fluorescence spectroscopy and two-dimensional correlation spectroscopy

Yun Kyung Lee ^a, Seongjin Hong ^b, and Jin Hur ^{a, *}

^a *Department of Environment and Energy, Sejong University, 209 Neungdong-ro, Gwangjin-gu, Seoul 05006, South Korea*

^b *Department of Ocean Environmental Sciences, Chungnam National University, Daejeon, 34134, South Korea*

* Corresponding author: Tel. +82-2-3408-3826. Fax +82-2-3408-4320.

E-mail: jinhur@sejong.ac.kr

5 tables: Tables S1 to S5

4 figures: Figs. S1 to S4

Table S1. Estimated numbers of MP pieces in the samples for leaching experiments using different plastic types.

Plastic type	MP concentrations in the mixture for designed leaching test	weight per piece	Number of MP pieces [†]
	(g-MP/L)	(mg/piece-MP)	(piece-MP/L)
PP (Density: 895-920 kg/m ³)		3.8	Approx. 1,316
PVC (Density: 1300-1450 kg/m ³)	5	7.7	Approx. 649
EPS (Density: 11-32 kg/m ³)		0.1 [*]	Approx. 48,387

* The weight per EPS piece was calculated using a collection of 30 pieces due to the light weight.

† The calculated values are rounded to integer.

The information was used to compare the leached MP-DOM amount per piece in Fig. 1e.

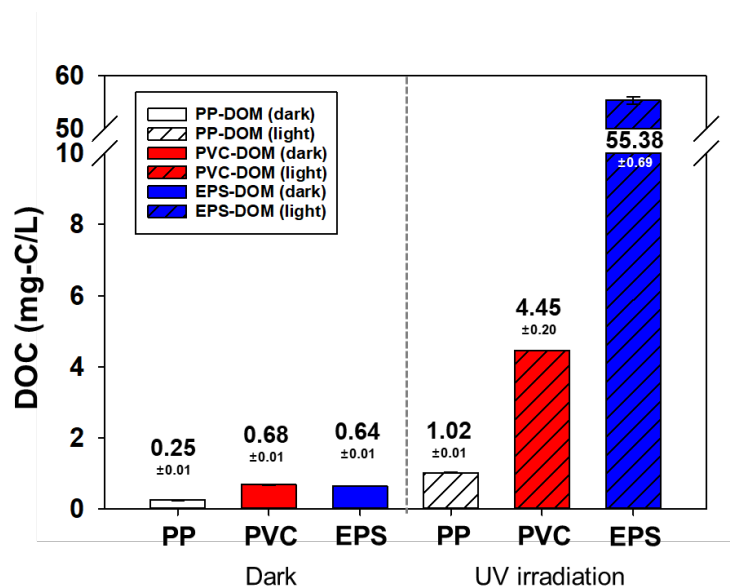
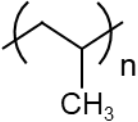
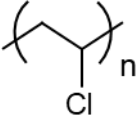
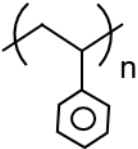


Figure S1. Leached DOC concentrations from PP, PVC, and EPS plastics after 14 days of leaching (5 g-MP/L) under dark and UV irradiation conditions.

Table S2. Main adsorption bands in the FTIR spectra of plastic (PP, PVC, and EPS plastics) particles and the leached MP-DOM, and their group assignments for identification.

Used plastic type	Chemical structure	Absorption bands (cm ⁻¹)	Assignment band used for identification	Bands reported in literatures (plastic type)		
Polypropylene (PP)		2921-2953 ^{P,D,L}				
		2915 ^P	A	C-H stretch	(Jung et al., 2018) – PP, PE, EPS	
		2835-2850 ^{P,D,L}				
		1602 ^L	B	C=C stretch	(Jung et al., 2018) - Nitrile	
		1454 ^{P,D,L}	C	CH ₂ bend	(Jung et al., 2018) - PP	
		1376 ^P	D	CH ₃ bend	(Jung et al., 2018) - PP	
		1253 ^D	E	CH bend	(Noda et al., 2007) - PVC	
		1096 ^{D,L}	F	C-C stretch	(Noda et al., 2007) - PVC	
		Various rock related with PP (1167-810)				(Jung et al., 2018) - PP
		1167 ^P		CH ₃ rock, C-C stretch		
		998 ^P		CH ₃ rock, CH ₃ bend, CH bend		
		968-972 ^{P,D}	G	CH ₃ rock, C-C stretch		
		842 ^P		CH ₂ rock, C-CH ₃ stretch		
		810 ^P		CH ₂ rock, C-C stretch		
Polyvinyl chloride (PVC)		2960 ^P				
		2928-2930 ^{P,D,L}	A'	C-H stretch	(Jung et al., 2018) – PP, PE, EPS	
		2855-2865 ^{P,D,L}				
		1739 ^L	B'	C=O stretch	(Lucki and Rånby, 1979)-EPS Carbonyl groups in photo-oxidized PS	
		1575 ^D	C'	COO stretch	(Bodecchi et al., 2005) - PVC Ca/Zn/Pb carboxylates used as heat stabilizers in PVC	
		1493 ^D	D'	BPA	(Wawrzyn et al., 2012) – BPA	
		1457 ^P	E'	CH ₂ bend	(Jung et al., 2018) - PVC	
		1334-1383 ^{P,L}	F'	CH bend	(Jung et al., 2018) - PVC	
		1253-1265 ^{P,D}				
		1172 ^L	G'	C-O stretch	(Gugumus, 1999) – Oxidized PE	
		1107 ^P	H'	C-C stretch	(Jung et al., 2018) - PVC	
		1055 ^D	I'	C-O-C stretch	(Passos et al., 2015) - PE	
960 ^P	J'	CH ₂ rock	(Jung et al., 2018) - PVC			
Expanded polystyrene (EPS)		3024 ^P	A''	CH ring stretch	(Jung et al., 2018) – EPS	
		2922-2932 ^{P,D,L}	B''	C-H stretch	(Jung et al., 2018) – PP, PE, EPS	
		2847-2858 ^{P,D,L}				
		1745 ^L	C''	C=O stretch	(Lucki and Rånby, 1979)-EPS Carbonyl groups in photo-oxidized PS	
		1643-1648 ^{D,L}	D''	C=C stretch	(Yang and Zhang, 2004)-PS Monomer of PS	
		1544 ^L	E''	COO stretch	(Bodecchi et al., 2005) - PVC Ca/Zn/Pb carboxylates used as heat stabilizers in PVC	
		1600 ^P	F''	Aromatic ring stretch	(Jung et al., 2018) - EPS	
		1491-1498 ^{P,D}				
		1449-1456 ^{P,L}	G''	CH ₂ bend	(Jung et al., 2018) - PVC	
1020-1030 ^{P,L}	H''	Aromatic CH bend	(Jung et al., 2018) - PVC			

P : MP powder, D : MP-DOM in the dark, L : MP-DOM under UV irradiation condition
Letters can be cross referenced to bands shown in FT-IR spectrum in Figure 1a to 1c.
Letter for PP, Letter' for PVC, and Letter'' for EPS

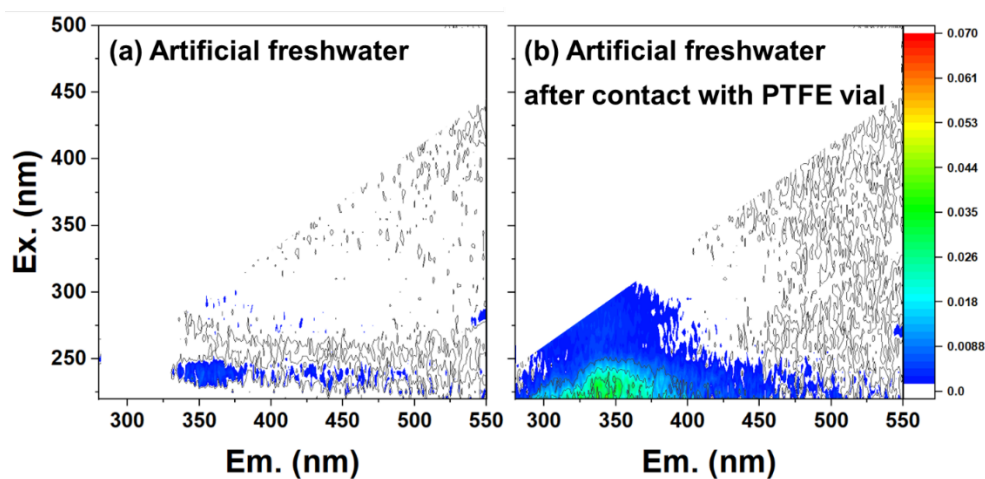


Figure S2. Fluorescence EEM plots of the artificial freshwater solutions used as a background before and after contact with polytetrafluoroethylene (PTFE) vial. Note that the scales of the EEM plots are same as those in Figure 2.

Table S3. Excitation and emission maxima of the fluorescent components of the plastic-derived DOM (validated by PARAFAC), their assignments, and the comparison with previous literatures.

Components	Ex	Em	Assignments (Labeled by Coble (1996))	Literature Comparison
C1	265(325)	463	(Terrestrial) Humic-like (Combination of traditionally defined peak A and C)	C1: <260/440 [Porewater] (Chen et al., 2017)
				C1: 240(345)/462 [Soil, Leaf] (Garcia et al., 2018)
				C1: 260(350)/470 [Soil] (Sharma et al., 2017)
				C7: 275/326 [Wetland] (Yamashita et al., 2010)
C2	250(325)	324	(Plastic-derived) Phenol/Protein-like (Combination of traditionally defined peak B and T)	C2: 275/345 [Leaf leachate] (Wheeler et al., 2017)
				C4: 280/335 [River] (Brogi et al., 2020)
				C2: 290(235)/410 [Plastic] (Lee et al., 2020)
C3	295(250)	411	Photo-induced Humic-like (Marine or microbial humic-like substance, Traditionally defined peak M)	C2: 305(<260)/414 [River] (Lambert et al., 2016)
				C1: 305(<250)/408 [River] (Brogi et al., 2020)
				C2: 310(<250)/400 [Lake] (Kothawala et al., 2014)

The comparison is based on the similarity >94 % obtained using the OpenFluor database.

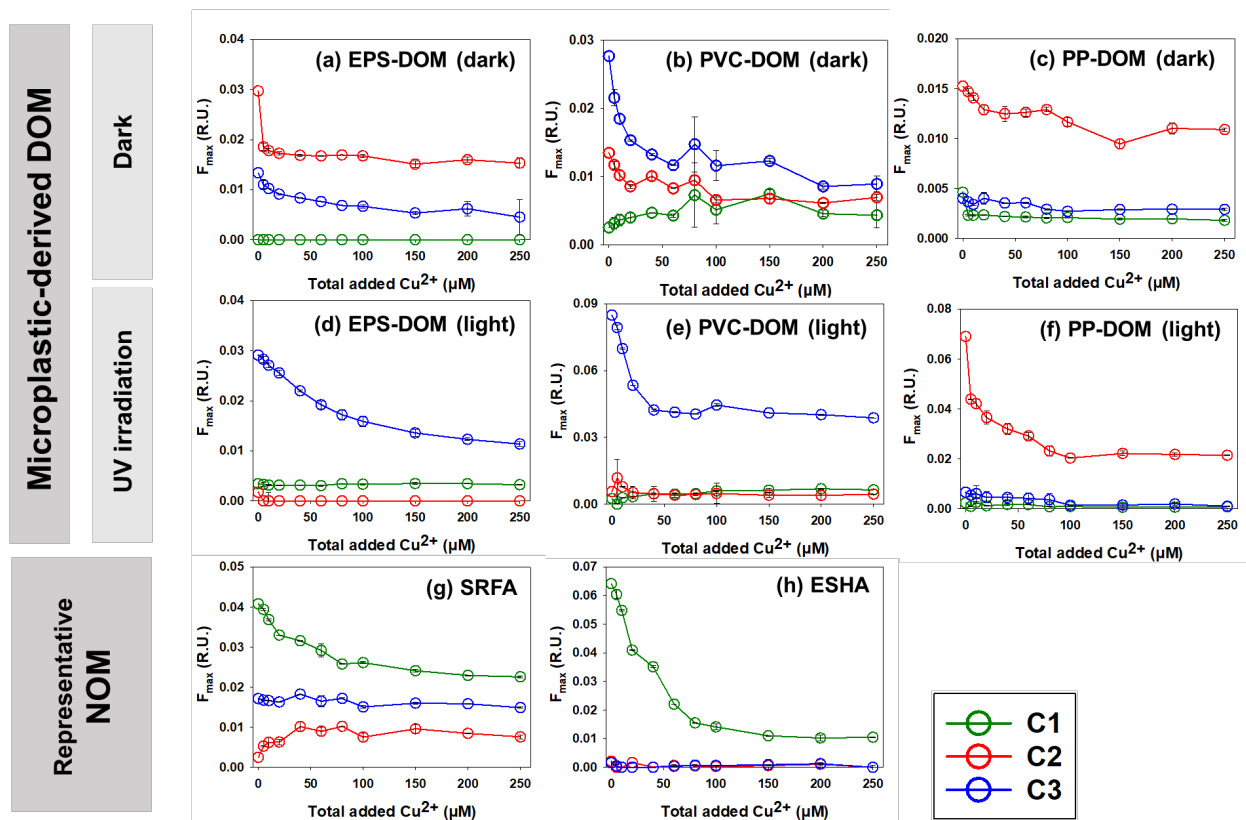


Figure S3. Changes in the F_{max} values of the individual components of SRFA, ESHA and MP-DOM under dark and UV irradiation conditions with increasing copper concentrations (from 5 to 200 $\mu\text{mol/L}$). The experimental condition is the same for MP-DOM and NOM samples.

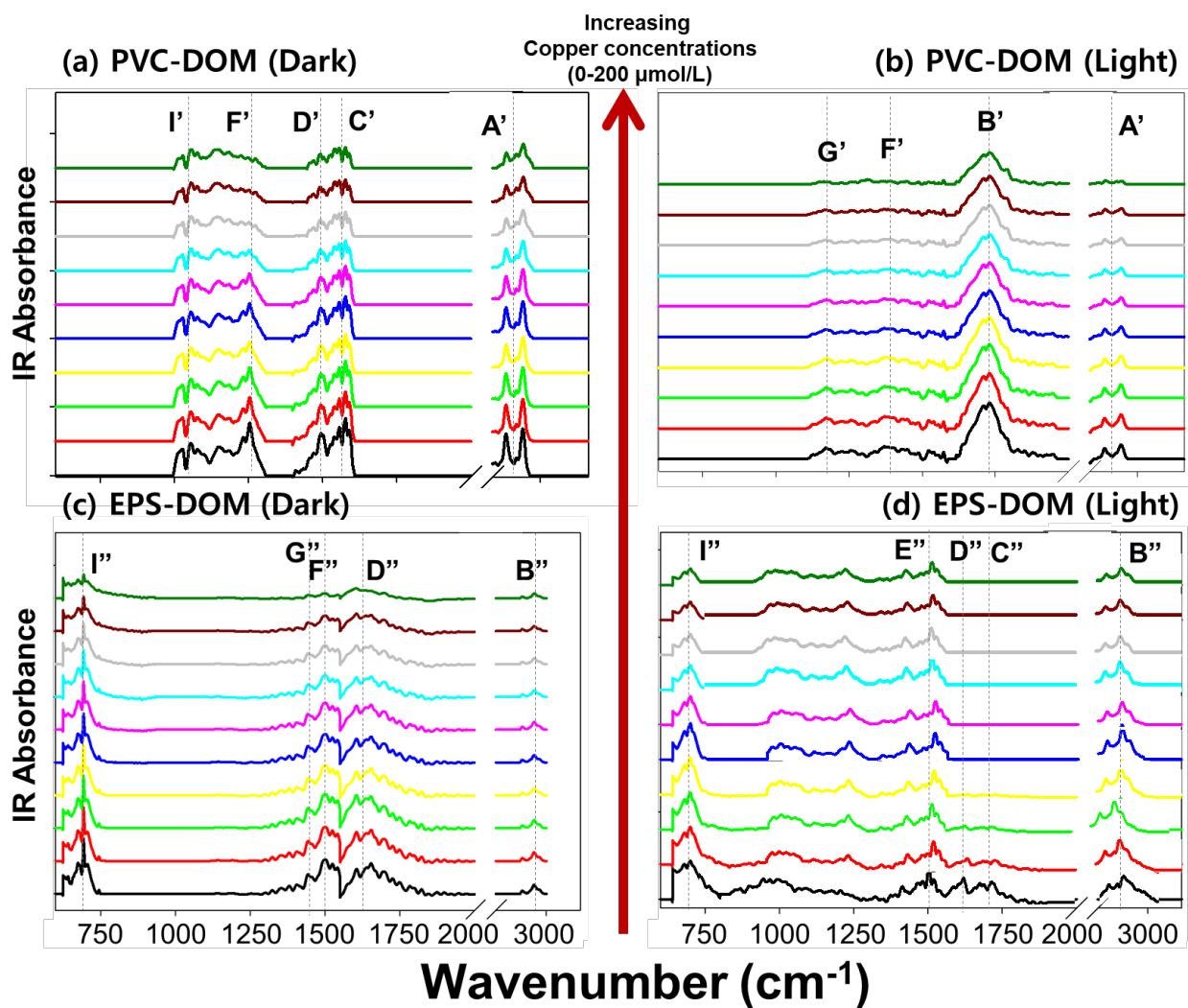


Figure S4. Changes in the FTIR spectra of PVC-DOM (a and b) and EPS-DOM (c and d) in the 600–3200 cm^{-1} region with increasing copper concentrations (from 5 to 200 $\mu\text{mol/L}$) under dark (a and c) and UV irradiation (b and d).

Table S4. Signs of cross-peaks (synchronous/asynchronous) in the asynchronous map of PVC-DOM with increasing copper concentration under the dark and the UV irradiation conditions.

		X-axis						
Y-axis		F'	D'	C'	B'	A'		
PVC-DOM (Dark)	F' (1255)	C-H bend		(++) 1.1E-13	(++) 1.3E-13			
	D' (1498)	Related with BPA			(+) 7.3E-14	No signal		
	C' (1575)	COO stretch						
PVC-DOM (Light)	F' (1371)	C-H bend		No signal		(++) 8.1E-14	(-) -1.0E-14	
	B' (1729)	C=O stretch					(- -) -7.8E-14	
	A' (2931)	C-H stretch						

(+), (-) : Positively and negatively signed cross peaks below the diagonal of the map over the FTIR range corresponding to the positive region of the synchronous map.
The bold letters refer to the cross peaks with the highest intensity in asynchronous map and marked with a red dotted line in Figure 5.

Table S5. Signs of cross-peaks (synchronous/asynchronous) in the asynchronous map of EPS-DOM with increasing copper concentration under the dark and the UV irradiation conditions.

		X-axis	I''	G''	F''	D''	C''	B''
Y-axis								
EPS-DOM (Dark)	I'' (702)	Aromatic CH bend		(-) -1.5E-09	(- -) -5.5E-09	(- -) -4.6E-09		
	G'' (1450)	CH ₂ bend			(+) 4.2E-10	(+) 1.7E-10		
	F'' (1500)	Aromatic ring stretch				(-) -2.9E-10	No signal	
	D'' (1653)	C=C stretch						
EPS-DOM (Light)	I'' (702)	Aromatic CH bend		No signal		(- -) -3.0E-08	(++) 2.7E-08	(- -) -4.1E-08
	D'' (1648)	C=C stretch					(+) 1.3E-10	(-) -5.8E-09
	C'' (1742)	C=O stretch						(-) -4.9E-09
	B'' (2915)	C-H stretch						

(+), (-) : Positively and negatively signed cross peaks below the diagonal of the map over the FTIR range corresponding to the positive region of the synchronous map.

The bold letters refers to the cross peaks with the highest intensity in asynchronous map and marked with a red dotted line in Figure 5.

References

- Bodecchi, L.M., Cocchi, M., Malagoli, M., Manfredini, M. and Marchetti, A. (2005) Application of infrared spectroscopy and multivariate quality-control methods in PVC manufacturing. *Analytica chimica acta* 554(1-2), 207-217.
- Brogi, S.R., Balestra, C., Casotti, R., Cossarini, G., Galletti, Y., Gonnelli, M., Vestri, S. and Santinelli, C. (2020) Time resolved data unveils the complex DOM dynamics in a Mediterranean river. *Science of The Total Environment*, 139212.
- Chen, M., Kim, S.-H., Jung, H.-J., Hyun, J.-H., Choi, J.H., Lee, H.-J., Huh, I.-A. and Hur, J. (2017) Dynamics of dissolved organic matter in riverine sediments affected by weir impoundments: Production, benthic flux, and environmental implications. *Water research* 121, 150-161.
- Garcia, R.D., Diéguez, M.d.C., Gereá, M., Garcia, P.E. and Reissig, M. (2018) Characterisation and reactivity continuum of dissolved organic matter in forested headwater catchments of Andean Patagonia. *Freshwater Biology* 63(9), 1049-1062.
- Gugumus, F. (1999) Formation of ester functional groups in oxidizing polymers. *Polymer degradation and stability* 65(1), 5-13.
- Jung, M.R., Horgen, F.D., Orski, S.V., Rodriguez, V., Beers, K.L., Balazs, G.H., Jones, T.T., Work, T.M., Brignac, K.C. and Royer, S.-J. (2018) Validation of ATR FT-IR to identify polymers of plastic marine debris, including those ingested by marine organisms. *Marine pollution bulletin* 127, 704-716.
- Kothawala, D.N., Stedmon, C.A., Müller, R.A., Weyhenmeyer, G.A., Köhler, S.J. and Tranvik, L.J. (2014) Controls of dissolved organic matter quality: Evidence from a large-scale boreal lake survey. *Global change biology* 20(4), 1101-1114.
- Lambert, T., Bouillon, S., Darchambeau, F., Massicotte, F. and Borges, A.V. (2016) Shift in the chemical composition of dissolved organic matter in the Congo River network. *Biogeosciences* 13(18), 5405-5420.
- Lee, Y.K., Murphy, K. and Hur, J. (2020) Fluorescence signatures of dissolved organic matter leached from microplastics: Polymers and additives. *Environmental science & technology*.
- Lucki, J. and Rånby, B. (1979) Photo-oxidation of polystyrene—Part 2: Formation of carbonyl groups in photo-oxidised polystyrene. *Polymer degradation and stability* 1(3), 165-179.
- Noda, I., Dowrey, A., Haynes, J. and Marcott, C. (2007) *Physical properties of polymers handbook*, pp. 395-406, Springer.
- Passos, T.M., Marconato, J.C. and Franchetti, S.M.M. (2015) Biodegradation of films of low density polyethylene (LDPE), poly (hydroxibutyrate-co-valerate)(PHBV), and LDPE/PHBV (70/30) blend with *Paecilomyces variotii*. *Polímeros* 25(1), 29-34.
- Sharma, P., Laor, Y., Raviv, M., Medina, S., Saadi, I., Krasnovsky, A., Vager, M., Levy, G.J., Bar-Tal, A. and Borisover, M. (2017) Green manure as part of organic management cycle: Effects on changes in organic matter characteristics across the soil profile. *Geoderma* 305, 197-207.
- Wawrzyn, E., Schartel, B., Seefeldt, H., Karrasch, A. and Jaeger, C. (2012) What reacts with what in

bisphenol A polycarbonate/silicon rubber/bisphenol A bis (diphenyl phosphate) during pyrolysis and fire behavior? *Industrial engineering chemistry research* 51(3), 1244-1255.

Wheeler, K., Levia, D. and Hudson, J. (2017) Tracking senescence-induced patterns in leaf litter leachate using parallel factor analysis (PARAFAC) modeling and self-organizing maps. *Journal of Geophysical Research: Biogeosciences* 122(9), 2233-2250.

Yamashita, Y., Scinto, L.J., Maie, N. and Jaffé, R. (2010) Dissolved organic matter characteristics across a subtropical wetland's landscape: application of optical properties in the assessment of environmental dynamics. *Ecosystems* 13(7), 1006-1019.

Yang, X. and Zhang, Y. (2004) Encapsulation of quantum nanodots in polystyrene and silica micro-/nanoparticles. *Langmuir* 20(14), 6071-6073.